

A model for particulate contaminated glow discharges

Michael J. McCaughey and Mark J. Kushner

University of Illinois, Department of Electrical and Computer Engineering, 1406 W. Green Street, Urbana, Illinois 61801

(Received 20 December 1990; accepted for publication 13 February 1991)

Glow discharges are often contaminated by particulates resulting from gas phase nucleation or sputtering of surfaces in contact with the plasma. If these particulates are sufficiently large, they will negatively charge and act as Coulomb-like scattering centers for electrons. In doing so, rate coefficients for high-threshold processes such as ionization may be reduced compared to those in pristine plasmas. If the contamination is nonuniform, then the resulting spatial irregularities in the rates of excitation may lead to plasma properties which are also nonuniform. In this paper, we report on the results of a model for argon glow discharges contaminated by dust. Rate coefficients for this model are generated by a separate Monte Carlo simulation of electron swarms in dusty plasmas. We find that under quasi-steady-state conditions, current flow and subsequent excitation of the gas are channeled into regions of lower dust density, and that these effects depend on the density, size, and distribution of the dust. In low pressure (< 10 Torr) glow discharges having similar dimensions, comparable perturbation in plasma properties due to contamination is obtained when $N_D P$ is approximately constant (N_D is the dust density, P is the gas pressure). The onset of perturbations may occur when $N_D P > 10^5 \text{ cm}^{-3} \text{ Torr}$.

I. INTRODUCTION

Although glow discharges are usually analyzed as being pristine plasmas, technologically relevant devices such as ion accelerators, lasers, plasma processing reactors, and magnetohydrodynamic power generators are routinely contaminated with gas phase particulates.¹⁻¹¹ These particulates, or "dust," result from gas phase nucleation, polymerization, or sputtering of electrode and wall surfaces. The sizes of the particulates are 10s of nm to 100s of microns.^{1,8-10} Particulate contaminated glow discharges, though generally not a desired method of operation, have been the object of many experimental studies in recent years.³⁻¹¹ The source of this interest has primarily been the deleterious effects that particulates are believed to have on the product in plasma material processing. For example, the quality of amorphous silicon films as used in thin-film photovoltaics degrades with the onset of gas phase polymerization.¹² Contamination of microelectronic devices by particulates during etching in plasma processing reactors significantly reduces the yield of the finished product and is now an important consideration in the design of etching equipment.¹³

Roth and Spears investigated the growth of particulates in radio frequency (rf) silane glow discharges using laser light scattering.⁵ They found that particles accumulated at the plasma sheath boundary, suggesting they are negatively charged. Wu and Miller confirmed this observation by measuring negatively charged particulates in the downstream plume of an rf discharge.¹⁴ Similar behavior was observed by Selwyn *et al.*^{3,4} in rf discharges sustained in CCl_2F_2 , Ar/Cl_2 and other mixtures, and by Jellum and Graves in dc and rf sputter discharges in Ar.^{6,8} The density of particulates in plasma processing reactors as used for the production of microelectronics devices has been estimated by laser light scattering. Values range as high as 10^5 - 10^8

cm^{-3} for particulate sizes ranging from 100s nm to 100s μm , with larger sizes having smaller densities.^{3,8-10} Steinbrüchel and co-workers collected particles having radii of 0.5 to a few microns in typical etching discharges, with clusters having many particles.^{15,16} Observations of the influence of dust in other discharge systems have been less quantitative but are equally problematic. For example, the presence of dust in high pressure CO_2 lasers¹⁷ and excimer lasers² has been correlated with the onset of instabilities such as arcing and streamers.

The presence of dust in glow discharges is certainly manifested by the effect it may have on the quality of the product, such as a deposited film, and these effects are quite specific to given systems. Dust, though, also influences glow discharges because it can significantly perturb electron transport. Dust which is sufficiently large, that is commensurate with the Debye length, λ_D , of the plasma, can be thought of as having a macroscopically large (electrically floating) dielectric surface. Due to the larger random flux of electrons compared to ions, floating bodies charge negatively to balance the flux of negative and positive charge carriers to their surfaces. The potential to which macroscopic surfaces charge is the floating sheath potential and is approximately

$$\phi_s \approx -\frac{kT_e}{2q} \ln\left(\frac{T_e M_I}{T_I M_e}\right), \quad (1)$$

where the subscripts e and I refer to electrons and ions, M is a mass, and T is a temperature. The extent of the negative potential surrounding the particles is a few Debye lengths.

Dusty plasmas in space have been studied in some detail.¹⁹⁻²¹ The conditions of those plasmas, though, are usually quite different from those in gas discharges. In particular, the Debye length in space plasmas is typically

larger than the distance between particles, whereas in gas discharges, the Debye length is typically smaller than the distance between particles. As a result, electrons in gas discharges most likely interact with each particle independently and collective effects are less important. There are, though, critical combinations of particle and plasma densities which can result in quasi-condensed phases of particulates.²²

In a previous study, we investigated the effects of dust contamination on electron transport coefficients under conditions where collective effects are not important.²³ We found that the electron energy distribution (EED) in dusty plasmas is a function of the number density and sizes of the particles, and that the EED in dusty plasmas is shifted to lower energies compared to the EED in a pristine plasma at the same E/N (electric field/gas number density). As a result, electron impact rate coefficients for high threshold processes, such as ionization, decrease in dusty plasmas, requiring a higher operating voltage to sustain the plasma.

Given this dependence of the EED, and hence rate coefficients, on particulate contamination, it is probable that discharges which are nonuniformly contaminated will themselves have nonuniform plasma parameters such as electron temperature, current density, or excited state densities. For example, a large disparity in rate coefficients for ionization caused by a nonuniform distribution of dust could lead to discharge instabilities at sufficiently high pressures. In this paper, we report on a computational study of the effects of particulate contamination on the structural properties of positive column glow discharges. These results were obtained from two coupled computer models. The first is a Monte Carlo simulation in which electron transport coefficients in dusty plasmas are obtained. The second is a two-dimensional model for positive column discharges in which the continuity equations are solved for charged and neutral species. Many of the technologically relevant discharges in which contamination is a concern are admittedly not positive columns. Individually addressing each of those systems, though, is beyond the scope of this work. The intent of this study is to derive threshold values of, for example, the density of dust at which the properties of the plasma are perturbed. With these scalings, one may then assess whether dust contamination in the particular discharge of interest may be a problem.

In Sec. II, the models we have used in our study will be described. The results of our study for contamination of positive column discharges in cylindrical bore discharges will be discussed in the following two sections. In Sec. III, one-dimensional distributions of contaminants will be considered, and in Sec. IV, two-dimensional distributions will be discussed. Our concluding remarks are in Sec. V.

II. DESCRIPTION OF THE MODELS

Our model of dusty discharge plasmas consists of two parts: a microscopic model and a macroscopic model. The processes of interest for the microscopic model are those which depend upon the interaction of electrons with dust particles having a spatial scale commensurate with the De-

bye length. Electron impact rate coefficients calculated with the microscopic model are used as input to the macroscopic model. The processes of interest for the macroscopic model are those which can be averaged over many dust particles, or on a spatial scale which is large compared to the Debye length.

A. Microscopic model

The microscopic model has been previously described²³ and so will only be briefly discussed here. The purpose of the microscopic model is to examine the perturbation of electron trajectories resulting from encounters with charged particulates. The model is a Monte Carlo-Molecular Dynamics hybrid which operates in the following fashion. Dust particles having a specified number density (N_D) and distribution of radii (r_D) are seeded in the plasma. The Debye length of the plasma is also specified. We assume that the particle has previously charged and that the potential in the Debye shielded volume around the particle is

$$\phi(r) = \frac{\phi_s r_D \exp[-(r - r_D)/\lambda_D]}{r}, \quad (2)$$

where ϕ_s is the sheath potential at the surface of the particle and r is the distance from the center of the particle. A value for E/N far from the particle is specified, the trajectories of electrons are initialized and the equations of motion of the electrons are advanced. Collisions of electrons with gas atoms are described using standard Monte Carlo techniques and null cross sections.²⁴ When an electron is far from a dust particle, it is accelerated by only the bulk E/N . Its trajectory is advanced in increments equal to its randomly selected time between collisions. When an electron nears a dust particle, its trajectory is perturbed by the electric field of the sheath surrounding the particle. At that time, molecular dynamics techniques are used to advance the particle through the sheath of the dust particle using Eq. (2) to obtain the local electric field. This portion of the program differs from the Monte Carlo portion in that small time steps must be taken in order to resolve the electric field. Collisions of electrons with gas atoms are allowed in the sheath. If an electron collides with a dust particle it is removed from the simulation. Statistics are periodically collected on the energy and location of electrons. From these statistics the EED is obtained either averaged over the volume of the plasma or as a function of distance from the particle.

The purpose of the sheath surrounding the dust particle is to balance the flux of electrons and ions to its surface.¹⁸ The expression for ϕ_s in Eq. (1) is obtained assuming that the EED is a Maxwellian and that the particle size is large compared to λ_D . The EED in the plasmas of interest, though, may not be a Maxwellian. The actual sheath potential of the dust used in the model is obtained by requiring a balance between the electron and ion fluxes to the surface of the particle. This balance is obtained by solving

$$\frac{n_I v_I}{4} \Gamma(r_D, \lambda_D) = \frac{n_e}{4} \int_{\phi_s}^{\infty} f(\epsilon) \left(\frac{2\epsilon}{m_e} \right)^{1/2} d\epsilon \quad (3)$$

for ϕ_s . In Eq. (3), n_I and n_e are the ion and electron densities, v_I is the thermal ion velocity, and $f(\epsilon)$ is electron energy distribution (eV^{-1}). Γ is the efficiency of the particle for collecting ions. This value can be approximated by viewing the particle as being a floating spherical probe having radius r_D . In this approximation, Eq. (29) of Ref. 25 may be used for Γ . If $r_D \gg \lambda_D$ the collection radius is the geometrical radius of the particle and $\Gamma = 1$. If $r_D \ll \lambda_D$ then Γ decreases from unity. The integral in Eq. (3) accounts for the fact that only electrons having an energy greater than the sheath potential may be collected by the particle.

B. The macroscopic model

The macroscopic model is a two-dimensional continuum simulation of a cylindrical positive column glow discharge. In this model the continuity equations for electrons, ions, and neutral particles are solved using electron impact rate coefficients obtained from the microscopic model. For example, the continuity equation for electrons is

$$\frac{\partial n_e}{\partial t} = \sum_j n_e N_i k_{ij} + \sum_j N_i N_j k_j + \nabla D \nabla n_e - \nabla \cdot \mu_e n_e \mathbf{E}, \quad (4)$$

where the first term accounts for ionization and recombination, the second term accounts for sources of electrons due to heavy particle collisions such as Penning ionization, and the last terms are for transport by diffusion and drift in the electric fields. For the cases of interest, diffusion is ambipolar and we use the local field approximation to obtain transport coefficients. The spatial derivatives are constructed using finite differences in cylindrical coordinates. The donor cell method is used to specify fluxes between computational cells. The boundary conditions are that all charged and excited state species densities vanish at the walls, and radial spatial derivatives are zero on the axis. The equations are integrated in time using a third order Runge-Kutta technique.

The local field approximation (LFA) assumes that the electron energy distribution can be characterized by quantities at the location of interest (e.g., electric field, excited state densities, gas mixture). The LFA is not valid when there are ballistic components to the EED, which is not the case here. The results of a companion study²⁶ of the radially resolved EED in cylindrical glow discharges indicate that the LFA is acceptable for the steady state when pd (pressure \times diameter) $\gtrsim 1.5$ Torr cm, which is commensurate with most of the cases of interest. For those cases where $pd \lesssim 1.5$ Torr cm, the local effects of dust contamination may be overestimated.

In the macroscopic model, the spatial scale of interest is large compared to λ_D , and therefore the space charge regions surrounding individual particles can be ignored in solving for the bulk electric field. In the model the local electric field is obtained by invoking current continuity and solving for the electric potential, ϕ , from

TABLE I. Reactions and rates included in the model.

Process	Rate coefficient ^{a,b}
$e + \text{Ar} \rightarrow \text{Ar}^+ + 2e$	c
$e + \text{Ar} \rightarrow \text{Ar}^* + e$	c
$e + \text{Ar} \rightarrow \text{Ar}^{**} + e$	c
$e + \text{Ar}^* \rightarrow \text{Ar}^+ + 2e$	$6.8 \times 10^{-9} T_e^{0.67}$
$e + \text{Ar}^* \rightarrow \text{Ar}^{**} + e$	$8.90 \times 10^{-7} T_e^{0.51}$ $\times \exp(-1.59/T_e)$
$e + \text{Ar}^{**} \rightarrow \text{Ar} + e$	c
$e + \text{Ar}_2^+ \rightarrow \text{Ar}^* + \text{Ar}$	$5.4 \times 10^{-8} T_e^{-0.66}$
$e + \text{Ar}_2^+ \rightarrow \text{Ar}^{**} + \text{Ar}$	$1.1 \times 10^{-7} T_e$
$e + \text{Ar}_2^+ \rightarrow 2\text{Ar} + e$	$1.0 \times 10^{-7} T_e$
$e + \text{Ar}_2^+ \rightarrow \text{Ar}_2^+ + 2e$	$9.0 \times 10^{-8} T_e^{0.70}$ $\times \exp(-3.66/T_e)$
$e + \text{Ar}^{**} \rightarrow \text{Ar}^+ + 2e$	$1.8 \times 10^{-7} T_e^{0.61}$ $\times \exp(-2.61/T_e)$
$2e + \text{Ar}^+ \rightarrow \text{Ar}^* + e$	$5.0 \times 10^{-27} T_e^{-4.5} (\text{cm}^6 \text{s}^{-1})$
$\text{Ar}^* + \text{Ar}^* \rightarrow \text{Ar}^+ + \text{Ar} + e$	5.0×10^{-10}
$\text{Ar}_2^+ + \text{Ar}_2^+ \rightarrow \text{Ar}_2^+ + 2\text{Ar} + e$	5.0×10^{-10}
$\text{Ar}^{**} + \text{Ar} \rightarrow \text{Ar}^* + \text{Ar}$	1.0×10^{-10}
$\text{Ar}^{**} + \text{Ar}^{**} \rightarrow \text{Ar}^+ + \text{Ar} + e$	5.0×10^{-10}
$\text{Ar}^+ + 2\text{Ar} \rightarrow \text{Ar}_2^+ + \text{Ar}$	$2.50 \times 10^{-31} (\text{cm}^6 \text{s}^{-1})$
$\text{Ar}^* + 2\text{Ar} \rightarrow \text{Ar}_2^+ + \text{Ar}$	$1.14 \times 10^{-32} (\text{cm}^6 \text{s}^{-1})$
$\text{Ar}_2^+ \rightarrow 2\text{Ar}$	$6.20 \times 10^7 (\text{s}^{-1})$

^aRate coefficients have units of $\text{cm}^3 \text{s}^{-1}$ unless otherwise noted. T_e is the electron temperature (eV).

^bRate coefficients were obtained from Ref. 28 unless otherwise noted.

^cRate coefficient is a function of E/N . See text Sec. II B.

$$\nabla j = -\nabla \sigma \nabla \phi = 0, \quad (5)$$

where j is the drift current density and σ is the conductivity. The boundary conditions are that no current flow to the walls and the radial electric field is zero on the axis. Equation (5) was solved using the method of successive-over-relation.²⁷

In this study, we examined glow discharges sustained in argon. The kinetic processes included in the model are given in Table I. The rate coefficients in Table I which are denoted as being functions of E/N were obtained in the following manner. The microscopic model was parameterized for N_D , λ_D , and E/N . The resulting transport coefficients were entered into a lookup table which was interpolated during execution of the model using local values of, for example, E/N . T_e is also a function of the interpolation parameters. Rate coefficients in Table I which are functions of electron temperature are therefore also indirectly obtained from the microscopic simulation by the dependence of T_e on E/N and N_D .

III. PARTICULATE CONTAMINATION IN CYLINDRICAL BORE DISCHARGES

Direct measurements of particulate size and densities in glow discharges are difficult but estimates have been made based on laser scattering and attenuation. Particulates having radii of a few hundred nm in discharges of < 1 Torr have been estimated to have densities of 10^6 – 10^8 cm^{-3} . Proportionally fewer particles occur with sizes of a few microns. To address these conditions, the particles in our study have radii of a few microns and the densities

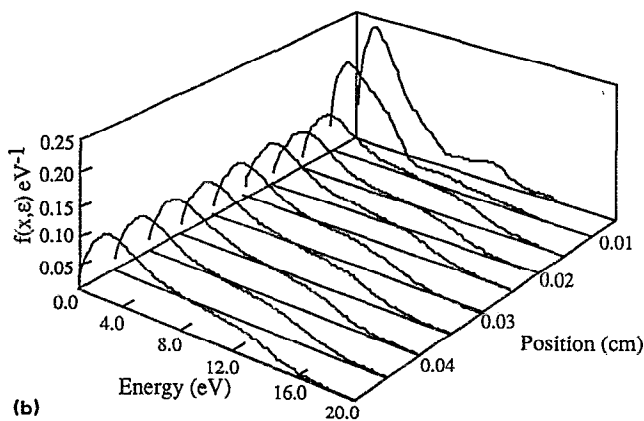
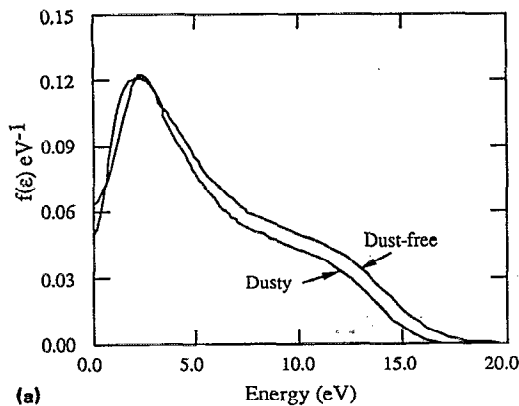


FIG. 1. The presence of dust in Ar discharges has damping effect on the electron energy distribution (EED), shown here for $E/N=7 \times 10^{-17}$ V cm² and a dust density of 10^5 cm⁻³ ($r_D=1 \mu\text{m}$). (a) EED averaged over the plasma compared to the EED for a pristine plasma; (b) EED in the vicinity of a dust particle. The EED is more critically damped close to the particle due to the negative potential in its surrounding sheath.

have 10^6 cm⁻³ as an upper limit. The effects we will discuss become more severe as the radii and density of the particles increase.

The effect of dust contamination on high-threshold energy transport coefficients, such as ionization, is manifested by a shift of the EED to lower energies with increasing dust density or radii of the dust. The EED averaged over the plasma with and without contamination is shown in Fig. 1(a). The gas is Ar, the particulate radius is $1 \mu\text{m}$, $N_D = 10^6$ cm⁻³, and the bulk E/N far from a particle is 7 Td ($1 \text{ Td} = 1 \times 10^{-17}$ V cm²). The EED, on an average basis, is shifted to lower energies thereby reducing rate coefficients for high threshold processes. The EED in the vicinity of the particle is more dramatically shifted to lower energies, a result of the negative potential in the Debye sphere surrounding it, as shown in Fig. 1(b). Although the encounter of a low energy electron with the potential surrounding a dust particle is energetically conservative, the encounter results in a large change in vector momentum. The shift in the EED is more a consequence of this change in momentum than the inelastic loss of energy resulting from the collection of high energy electrons.

Ionization rate coefficients for Ar as a function of dust

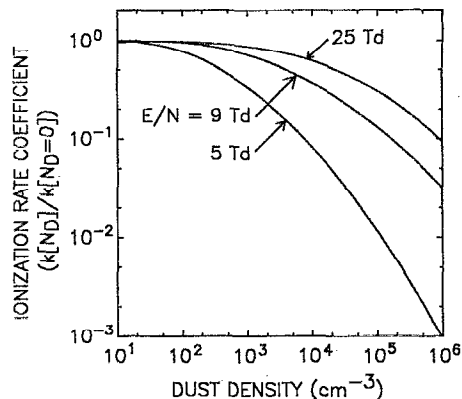


FIG. 2. The ionization rate coefficients for argon as a function of dust density normalized by their pristine values. The reduction of this coefficient with increasing dust is noticeably greater at lower E/N . This reduction is a result of the Coulomb-like scattering of electrons by dust particles, which scales inversely with energy.

density are shown in Fig. 2 for several values of E/N . These coefficients have been normalized by their pristine values to emphasize the effects of the dust. The average electron energies for the same conditions are shown in Fig. 3. Increasing dust densities result in lower rate coefficients for ionization, a result of the reduction of the high energy portion of the electron energy distribution. The average electron energy also decreases with increasing N_D , though the effect is less severe. The threshold dust density for which rate coefficients are significantly affected, 10^3 – 10^5 cm⁻³, decreases with decreasing E/N . The Coulomb-like potential surrounding the particulates effectively has a $1/\epsilon$ scaling for momentum transfer. Therefore, the difference in rate coefficients between pristine and dusty plasmas decreases as E/N , and the average electron energy, increases.

We next examine the effects of dust contamination uniformly distributed in cylindrical bore glow discharges. The discharge tube has a diameter of 1.5 cm with a filling pres-

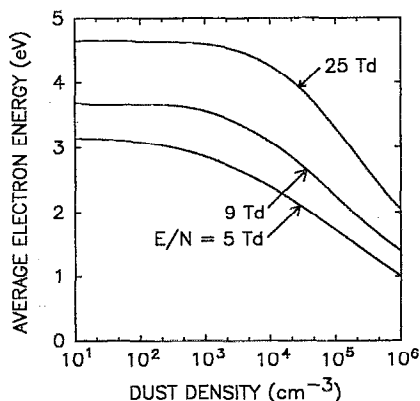


FIG. 3. The average electron energy in a dusty Ar discharge for the conditions of Fig. 2. The average electron energy decreases with increasing dust density and decreasing E/N , though to a lesser degree than the ionization rate coefficient. This indicates that the tail of the EED is more severely affected by contamination than the bulk distribution.

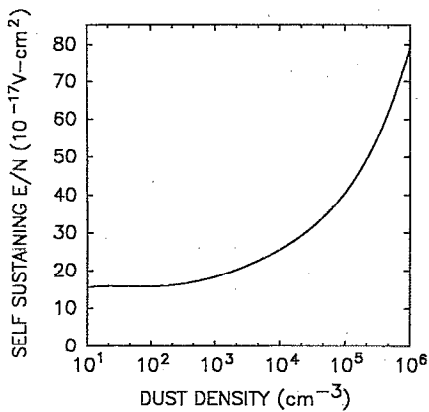


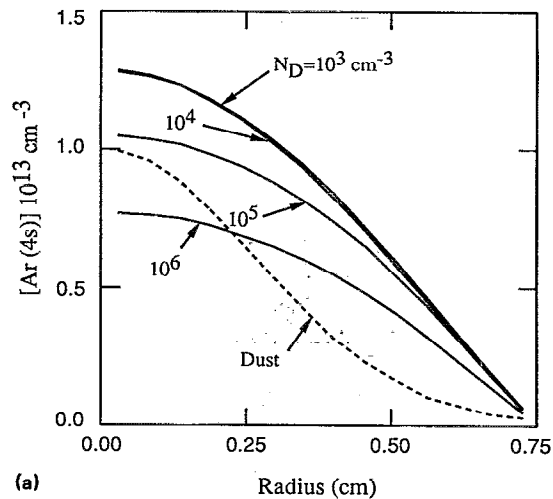
FIG. 4. The self-sustaining E/N in an Ar discharge as a function of dust density. The dust was uniformly distributed across the bore. The increase in E/N at higher dust densities is required to compensate the decrease in the rate coefficient for ionization and in the electron temperature.

sure of 0.1–10 Torr of Ar at 300 K. The discharge circuit parameters were chosen to provide a constant bore averaged current density of 8.5 mA/cm². In general, as the dust density increases, ionization rate coefficients decrease. Therefore a higher E/N is required to sustain the plasma, as shown in Fig. 4. These are, however, spatially stable discharges since the ionization rates are uniformly decreased.

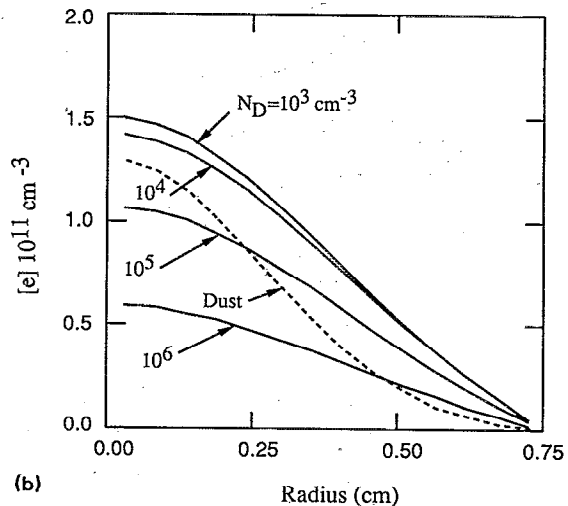
In conventional cylindrical bore discharges, the plasma potential is most positive on the axis and monotonically decreases towards the wall. Since the particles are negatively charged, their drift in the ambipolar field drives them towards the axis while diffusion convects them towards the wall. The particle distribution will markedly peak on the axis when

$$q_p \mu_p E_A > \frac{D_p}{\Lambda}, \quad E_A > \frac{kT_p}{\Lambda q_p} \quad (6)$$

where μ_p is the particle mobility, q is its charge, E_A is the ambipolar field, D_p is the particle diffusion coefficient, and Λ is the diffusion length of the discharge tube. Since E_A is typically a few V cm⁻¹ and $T_p \sim 300$ K, this inequality always holds. Dust particles should therefore normally be found near the axis of a positive column discharge. To simulate these conditions, particles were distributed in the tube using a Gaussian distribution centered on the axis. The Ar(4s), electron, and dust densities are shown in Fig. 5 for a gas pressure of 1.0 Torr for discharges with dust distributions having maximum densities of 10³–10⁶ cm⁻³. Due to the higher dust density near the axis, electron impact rate coefficients for excitation and ionization are lower there. As the dust density increases the densities of electrons and Ar(4s) atoms decrease on the axis relative to locations near the wall due to their lower production rates near the axis. Even though the production rates are significantly smaller at small radii, the high rate of diffusion at these pressures radially averages the effects of the dust, resulting in excited state densities more uniformly decreasing.



(a)



(b)

FIG. 5. The spatial distribution of the (a) Ar(4s) and (b) electron densities as a function of discharge radius for various dust densities. The gas pressure is 1 Torr and the average current density is 8.5 mA/cm². The dust profile is also shown. The large dust density at the center of the tube leads to a reduction of both the Ar(4s) and electron production rates. Diffusion averages the densities across the bore. A dust density of 10⁴ cm⁻³ begins to yield significant changes in excited state densities.

The reductions in electron density, and hence Ar(4s) density, seen in Fig. 5 are in part consequences of a disparity in the dependence of ionization rate coefficients and electron mobilities as a function of dust density. The circuit has been chosen so that the aperture averaged current density is a constant or $\langle n_e \mu_e E \rangle = \text{constant}$. The operational E/N increases with increasing N_D due to the decrease in average ionization coefficients. The electron mobility, though, is less sensitive to N_D , as shown in Fig. 6 where these values are plotted as a function of radius. The rate coefficient for ionization decreases towards the axis while the mobility, μ , is more nearly constant. (The increase in μ seen here near the axis is a consequence of the Ramsauer minimum in Ar, and is not a general result.) Since $n_e \sim 1/(\mu_e E)$ for constant current, then n_e will decrease with increasing N_D since E also increases. Jellum and Graves⁸

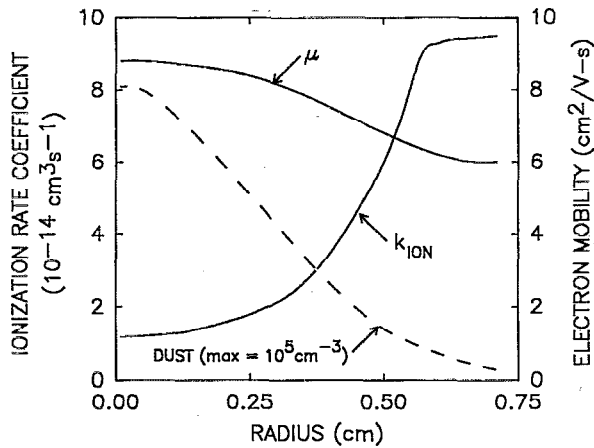
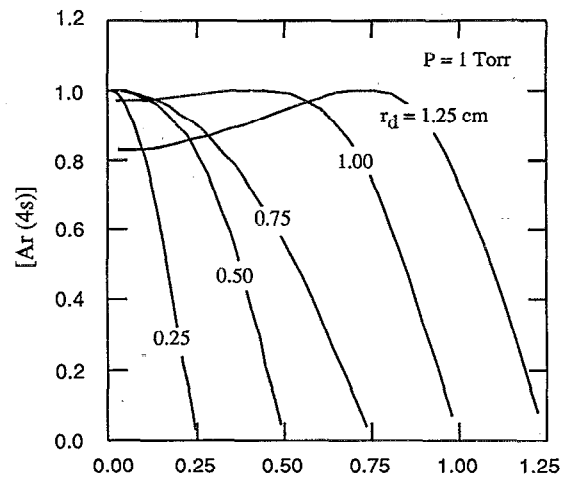


FIG. 6. Radial variations in the ionization rate coefficient and electron mobility for the dust profile shown and the conditions in Fig. 5. The ionization rate coefficient is more sensitive to the presence of dust than is the mobility. This leads to a decrease in $[e]$ when the current density is held constant. The increase in μ near the axis is a consequence of the Ramsauer minimum in argon and not a general result.

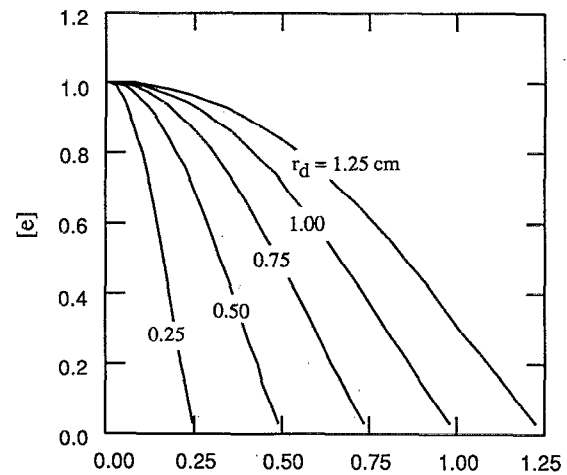
observed substantial decreases in both emission intensity and ion density in contaminated rf discharges in argon (0.5 Torr) as compared to pristine plasmas. Although the details of the dependence of emission and plasma densities on contamination will be functions of the circuit parameters, the trends observed by Jellum and Graves are consistent with our results.

The perturbations in the spatial distribution of Ar(4s) and of the electron density caused by nonuniform contamination are mitigated by two factors. First, if diffusion dominates, then the effects of nonuniform dust contamination will be averaged over the cross section of the tube. Second, in order for significant perturbations in the local density of a species to occur, there must be local processes which deplete its density. Otherwise, diffusion will compensate and "fill in" any lack of production of the species which would otherwise cause a local minimum in its density. Thus, the ratio of the diffusion length, or mean free path for loss of excited states and electrons, to the gradient length of the dust distribution (λ/L_D) is an important parameter in determining the spatial distribution of these species. As this ratio decreases, the spatial variation of electron and Ar(4s) densities will increase.

The ratio λ/L_D will, in general, decrease with increasing discharge tube radius. Increasing the gas pressure will also decrease λ/L_D by decreasing the diffusion length. To demonstrate these scalings, we parametrized the radius of the tube and gas pressure in the model. The resulting Ar(4s) and electron densities are plotted in Figs. 7 and 8 for similarly scaled dust profiles. The current density was maintained at an average of 8.5 mA/cm². The spatial distribution of Ar(4s) becomes markedly perturbed as the radius of the tube or pressure increase. $[Ar(4s)]$ decreases near the axis where the dust density is high, a trend which results from the Ar(4s) density dominantly being determined by local processes (excitation and superelastic re-



(a)



(b)

FIG. 7. The density of (a) Ar(4s) and (b) electrons as a function of radius for different diameters of the discharge tube. The densities are separately normalized by their maximum values. The maximum axial dust density is 10^6 cm^{-3} with $r_D = 1 \mu\text{m}$. As the diffusion length (λ) decreases relative to the dust gradient length, (L_D) more spatial variation in Ar(4s) is observed. The electron density does not show as severe a change since there are no local loss processes for electrons.

laxation) as opposed to transport when either the tube size or pressure is large. Under these conditions, the spatial variation in electron impact rate coefficients caused by the dust becomes more important in determining the spatial distribution of excited states.

The electron density, though, does not show significant perturbations in its spatial profile. This results from the diffusion length of electrons being larger than that for Ar(4s) and from there being no local loss processes for the electrons in low pressure positive column discharges. (Loss is dominated by diffusion.) In higher pressure discharges, dissociative recombination of dimer ions is an important local loss process, and nonuniformities in $[e]$ from particulate contamination are more likely. In electronegative plasmas attachment can be an important volumetric loss. The presence of dust, however, may itself be a loss process.

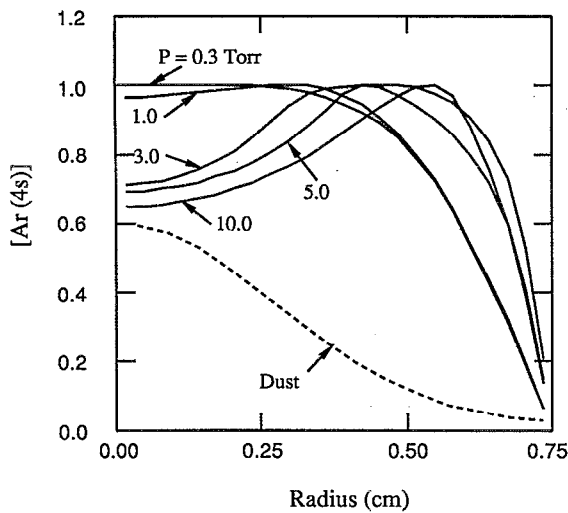


FIG. 8. Radial variation of the Ar(4s) density for different gas pressures normalized by their maximum values. The dust has a peak density of 10^5 cm^{-3} on the axis. Since λ/L_D decreases with increasing pressure, more severe perturbations are observed at the higher pressures.

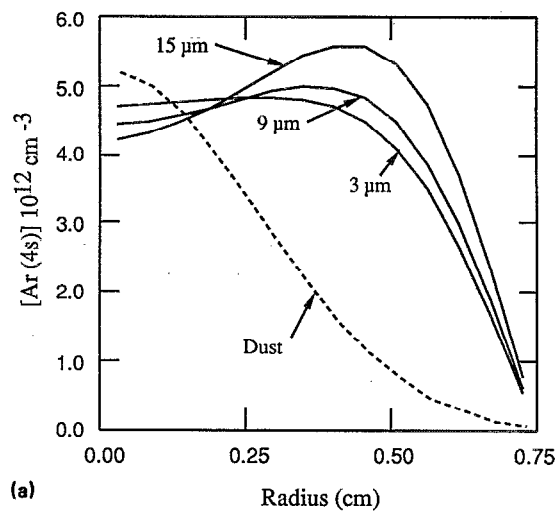
If a dust particle is large enough for a sheath to form at its surface, then the dust acts as a floating body in the plasma collecting equal fluxes of electrons and ions. The rate coefficient for collection of electrons and ions by dust is $k \approx \pi r_D^2 v_T$. For $N_D = 10^6 \text{ cm}^{-3}$ and $r_D = 2 \mu\text{m}$ the volumetric rate of loss of electrons and ions is $> 10^4 \text{ s}^{-1}$ for a unit collection efficiency. This is a rate which can be commensurate with both the rates of ionization and of diffusion.

To demonstrate the perturbation in the densities of electrons and excited states which could occur as a result of the collection of electrons and ions by dust, we included

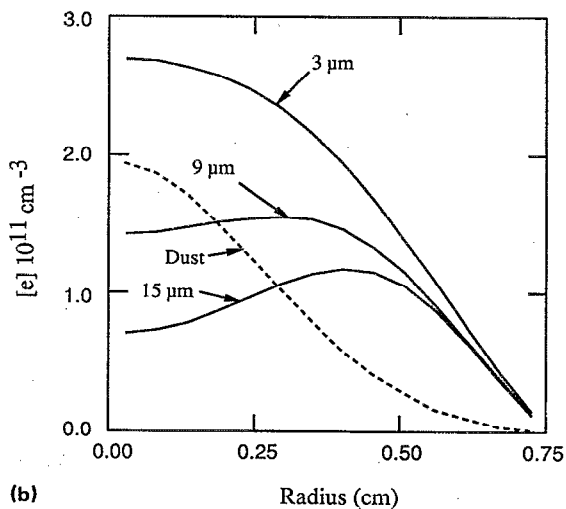


in the reaction scheme. The rate coefficient was $\pi r_D^2 v_T$. The results are shown in Fig. 9 for $N_D = 10^6 \text{ cm}^{-3}$ and $r_D < 15 \mu\text{m}$, and $P = 1 \text{ Torr}$. For dust radii greater than 3–5 μm , the local rate of collection exceeds the rate of ionization near the axis where the dust density is high and the discharge is not locally self-sustaining. There is a net loss of electrons near the axis and the electron density decreases there. There is a commensurate decrease in the Ar(4s) density.

To evaluate the possibility of particulate contamination causing instabilities in glow discharges, it is desirable to have scaling laws. The effects of increasing N_D are primarily manifested by the perturbation of electron impact rate coefficients. The effect of increasing gas pressure, P , is a reduction in the ability of diffusion to average spatial variations in electron impact rate coefficients caused by particulate contamination. To investigate the mutual scaling of N_D and P , we parametrized our model for $0.1 < P < 10 \text{ Torr}$ and $10^3 < N_D < 10^6 \text{ cm}^{-3}$. We found that similar degrees of nonuniformities in excited state densities were obtained when $N_D P \approx \text{constant}$. The threshold for significant perturbations is when this parameter exceeds 10^5 cm^{-3} .



(a)



(b)

FIG. 9. The density of (a) Ar(4s) and (b) electrons as a function of radius in the discharge for different radii of the dust ($N_D = 10^6 \text{ cm}^{-3}$) when collection of electrons and ions by the particles is included. The local loss of electrons causes perturbations in its density profile.

Torr. The threshold value will depend on the particular geometry, radii, and spatial distribution of the dust. The scaling, though, should approximately hold. For larger dust radii, collection effects begin to become important when $\lambda/(N_D \pi r_D^2) > 1$.

IV. EFFECTS OF NONUNIFORM PARTICULATE CONTAMINATION

The facts that particulates are negatively charged and have small diffusion coefficients result in dust accumulating in regions of positive plasma potential. The observation that particulates are often found adjacent to the sheaths or in the negative glow of discharges where the plasma potential has a local maximum is likely explained by the dominance of drift over diffusion in their transport. Particulates have also been observed to form large isolated islands where small perturbations in the electric potential presumably have formed local maxima in the plasma potential, thereby attracting the particles.³ Under specific conditions

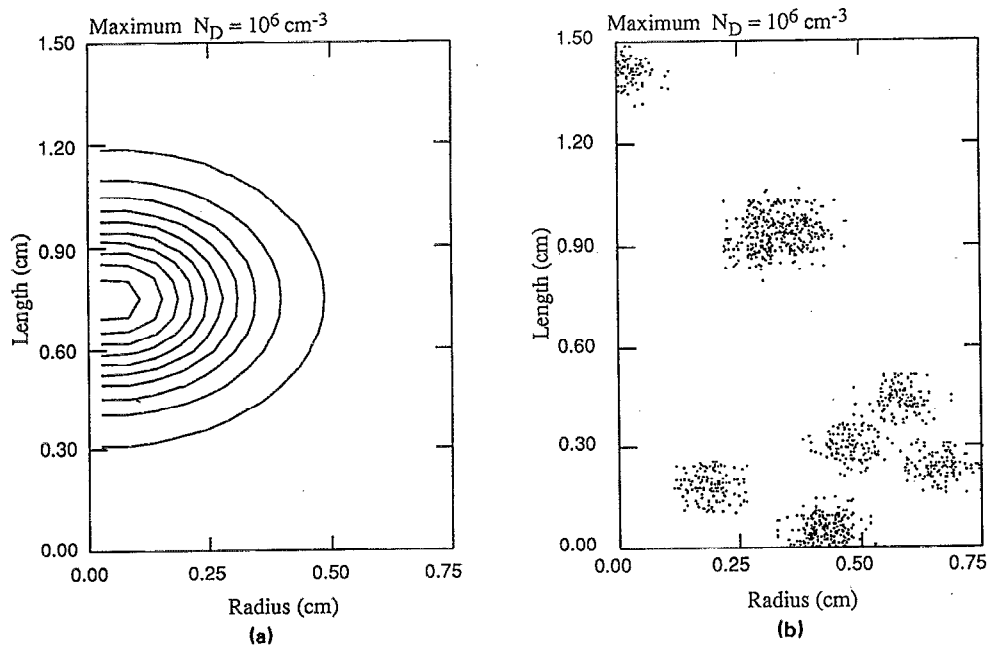


FIG. 10. Dust profiles used in the two-dimensional model as a function of radius and axial position. (a) Axial island of dust due to a local maximum in plasma potential; (b) random quasicondensed phases of particulates. The maximum value of dust density in each case is 10^6 cm^{-3} .

($0.3 < T_e < 3 \text{ eV}$, $10^3 < N_D < 10^6 \text{ cm}^{-3}$, $0.1 < r_D < 3 \mu\text{m}$), particulates may form quasicondensed phases which translate as rigid structures.²⁰

Given that particulates can cluster in isolated volumes of the plasma, we investigated the effects of there being islands of contamination on positive column glow discharges. In doing so, we simply specified that the dust have a given distribution to demonstrate the response of typical glow discharges to their presence. In this portion of our investigation we ran the model in a two-dimensional mode. The cylindrical positive column was divided into shorter axial segments having approximately a square aspect ratio. Periodic boundary conditions were applied to simulate a long positive column discharge.

We examined two distributions of dust, as shown in Fig. 10. The first configuration is the two-dimensional analog of the dust distributions discussed in the previous section. The dust has a radial Gaussian distribution with the density being highest on the axis, a likely distribution since the plasma potential in a positive column discharge is maximum on the axis. We further restricted the axial extent of the dust using a second Gaussian distribution, as shown in Fig. 10(a). The second distribution accounts for the possibility that particulates may form quasicondensed phases or accumulate in regions of shallow positive potential, conditions that could result in isolated islands of dust which are located somewhat randomly in the discharge. To simulate these conditions we randomly distributed islands of

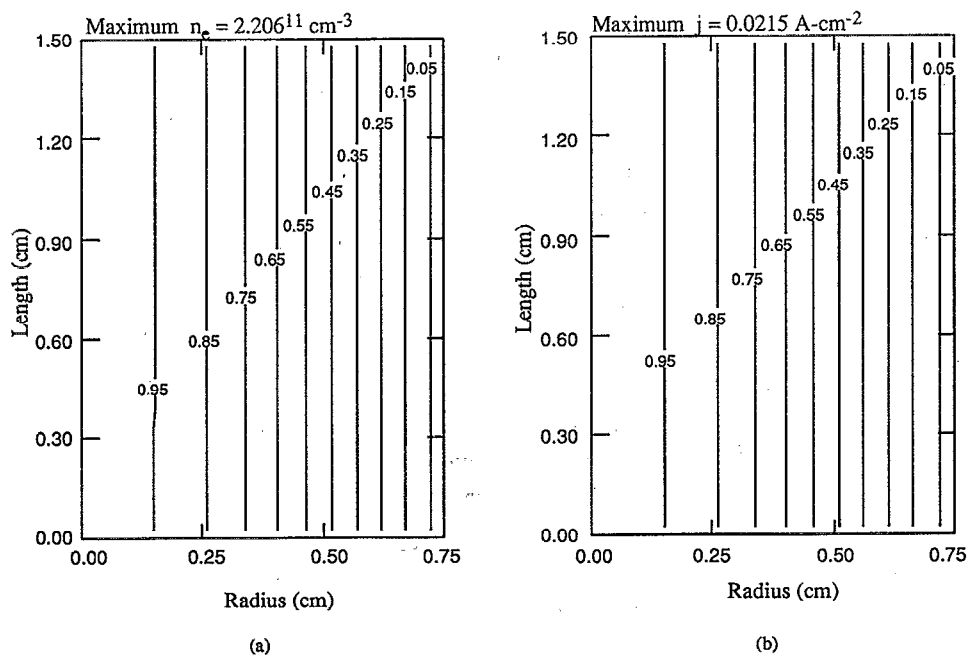


FIG. 11. Plasma parameters in the absence of dust: (a) electron density and (b) current density. The contours are labeled with their fractional value of the maximum density as noted at the top of the figure. In a pristine plasma, there are only radial variations in n_e and j .

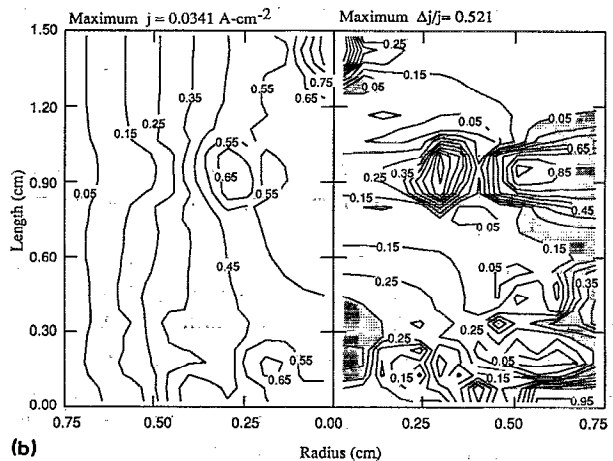
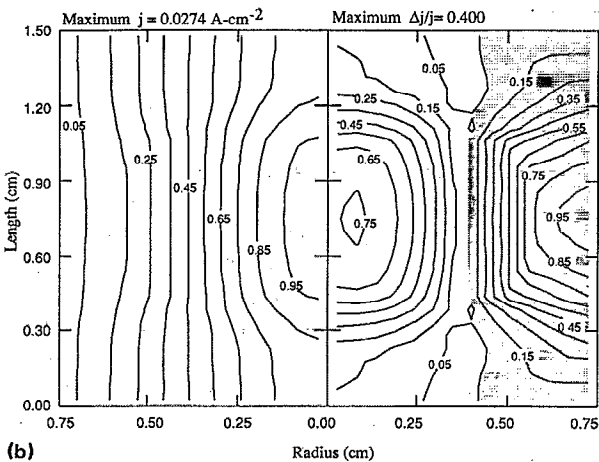
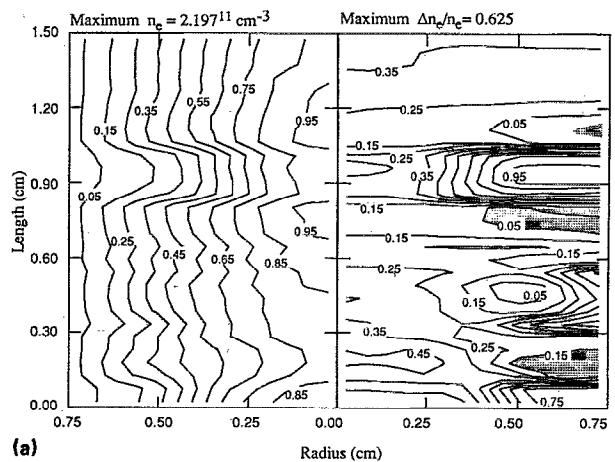
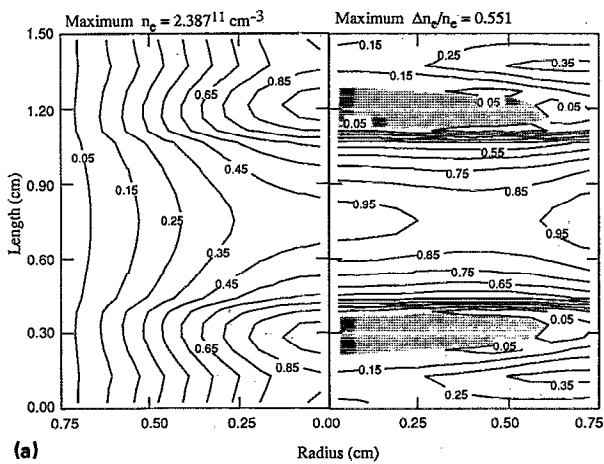


FIG. 12. Plasma parameters for dust contamination having the distribution shown in Fig. 10(a): (a) electron density and (b) current density. The actual density and relative change in density ($\Delta n/n = |n[N_D = 10^6 \text{ cm}^{-3}] - n[N_D = 0]|/n[N_D = 0]$) are shown. Grey regions show positive changes from their pristine values; clear areas are for negative changes. The contour labels are fractions of the maximum value noted at the top. The current density increases in the outer portion of the tube which is less contaminated.

dust in the discharge. Since our simulation is only two-dimensional, these islands are computationally represented as toroids. A representative distribution of dust is shown in Fig. 10(b).

For comparison, the electron and current densities in the absence of dust are shown in Fig. 11 where a 1.5 cm length of the discharge is shown. As one might expect, these densities have only radial variations. The electron and current densities, and their change compared to the pristine discharge, are shown in Fig. 12 for dust having a maximum value of 10^6 cm^{-3} and being distributed as shown in Fig. 10(a). The shaded regions show where either j or n_e increase compared to the pristine case. Since the circuit parameters have been chosen for constant current operation, the radially integrated current density at any axial location must be constant. Due to the reduction in the rate of electron impact ionization in regions contaminated by dust, the electron and current densities decrease

FIG. 13. Plasma parameters for dust contamination having the distribution shown in Fig. 10(b), (a) electron density and (b) current density. The labeling scheme is the same as Fig. 12. The islands of dust channel current into less contaminated regions.

in those regions. Since, however, the total current at any axial location must be conserved the current constricts to the outer portion of the tube, increasing there relative to the pristine case. The current effectively channels itself around the high impedance region generated by the dust on the axis. The distance over which the plasma responds to the presence of the dust can be many times the physical extent of the dust on the axis. The electron density decreases by $\approx 50\%$ in the central region which is heavily contaminated by dust, while the current density decreases by 30%. In the outer portion of the discharge tube, the current density increases by as much as 40% above its pristine value. The electron density increases ahead and behind the dust, but by only a few percent.

The electron and current densities, and the change from their pristine values, are shown in Fig. 13 for the random coalescences of dust. The trends are similar to those seen for the more uniform distribution of dust. The channeling effect of the dust on the current density is clearly shown. Again, due to the constant current conditions and the required increase in operating E/N to sustain

the plasma, the majority of the relative changes in electron density are negative. The local current density again decreases in heavily contaminated regions, and increases elsewhere. The local excursions in current density are as high as 50%.

Although not quantitatively addressed in this work, the nonuniform distributions of current density wrought by the presence of dust are ultimately not stable structures. The increase in current density in weakly contaminated regions compared to highly contaminated regions results in a higher rate of momentum transfer to the gas. If thermal conduction is the dominant form of heat transfer, the gas will locally heat. This heating generates a pressure gradient which will rarify a channel, resulting in a locally high value of E/N . Under quasi-cw conditions, there is additional gas heating due to the locally high value of E/N , causing more rarification. These conditions are unstable and eventually result in arcing. The likelihood that particulate contamination results in constriction and eventual arcing increases with increasing gas pressure and increasing size of the plasma tube, since this reduces the rate of conductive heat transfer. These are also conditions which increase the effects of particulate contamination. These observations may explain the acute sensitivity that high pressure discharges, such as excimer and CO_2 lasers,^{2,17} display to particulate contamination while low pressure devices such as plasma processing reactors can operate stably for long periods of time at the same or higher fractional levels of contamination.

V. CONCLUDING REMARKS

The influence of particulate contamination on positive column glow discharges has been theoretically investigated. We found that particulates reduce the rate coefficients for ionization and processes having high inelastic thresholds. The correlation between particulate contamination and discharge nonuniformities results from the ability for particulates to "direct" current flow into and through less contaminated regions. If the particles are non-uniformly distributed, constriction of the current may occur, a condition which is the precursor to arcing in high pressure discharges. Simple scaling laws have been proposed to predict the influence of dust in contaminated discharges. Systems in which the ratio of the excited state or electron diffusion or loss length to the gradient of the dust is small are more likely to have large variations in electron and excited state densities. Similar effects are obtained when $N_D P$ is constant. A value of $N_D P \approx 10^5 \text{ cm}^{-3} \text{ Torr}$ is approximately the threshold at which significant perturbation of the discharge occurs in plasmas of < 10 Torr pressure. For larger radii of dust, collection of charge carriers by the particles causes nonuniformities when $\Lambda / (N_D \pi r_D^2) > 1$.

Note added in proof. Recent work by the authors²⁹ and collaborators³⁰ has shown that distributions of dust in glow discharges can be significantly perturbed by momentum transfer from ions. This force pushes dust particles in the direction of the net ion flux and can, in some cases, dominate over the force of electrostatic trapping. Since the net

ion flux in positive column discharges is directed towards the wall, the effects of ion drag may force dust away from the axis where the potential is most positive. The methodology and conclusions discussed in this paper are not changed by these new findings.

ACKNOWLEDGMENTS

The authors thank Professor David Graves for his advice and his pointing out the possibility of having condensed phases of particulates and Dr. Gary Selwyn for his comments. This work was supported by the National Science Foundation (CBT88-03170 and ECS88-15781), and by IBM East Fishkill facility.

- ¹V. I. Donin and Yu. I. Khapov, *Sov. J. Quantum Electron.* **16**, 1034 (1986).
- ²G. V. Karachevtsev and A. A. Friedman, *Sov. Phys. Tech. Phys.* **21**, 1386 (1976).
- ³G. S. Selwyn, J. E. Heidenreich, and K. L. Haller, *Appl. Phys. Lett.* **57**, 1876 (1990).
- ⁴G. S. Selwyn, J. Singh, and R. S. Bennet, *J. Vac. Sci. Technol. A* **7**, 2758 (1989).
- ⁵R. M. Roth, K. G. Spears, G. D. Stein, and G. Wong, *Appl. Phys. Lett.* **46**, 235 (1985).
- ⁶G. M. Jellum and D. B. Graves, *J. Appl. Phys.* **67**, 6490 (1990).
- ⁷K. Spears, T. M. Robinson, and R. Roth, *IEEE Trans. Plasma Sci.* **14**, 179 (1986).
- ⁸G. M. Jellum and D. B. Graves, *Appl. Phys. Lett.* **57**, 2077 (1990).
- ⁹K. G. Spears, R. P. Kampf, and T. J. Robinson, *J. Phys. Chem.* **92**, 5297 (1988).
- ¹⁰K. R. Stalder, *Proc. SPIE* **1185**, 164 (1989).
- ¹¹E. W. Gray, *J. Appl. Phys.* **59**, 3709 (1986).
- ¹²W. Siefert, *Thin Solid Films* **120**, 267 (1984).
- ¹³A. R. Reinberg, in *Plasma Etching*, edited by D. M. Manos and D. L. Flamm (Academic, Boston, 1989), Chap. 5.
- ¹⁴R. J. Wu and R. J. Miller, *J. Appl. Phys.* **67**, 1051 (1990).
- ¹⁵J. L. Petrucci and Ch. Steinbrüchel, *Proceedings of 8th Symposium on Plasma Processing*, Electrochemical Society, 1990.
- ¹⁶J. A. Durham and Ch. Steinbrüchel, *Proceedings of 8th Symposium on Plasma Processing*, Electrochemical Society, 1990.
- ¹⁷C. Fisher (private communication).
- ¹⁸M. Mitchner and C. H. Kruger, *Partially Ionized Gases* (Wiley, New York, 1973), pp. 126-134.
- ¹⁹E. C. Whipple, T. G. Northrup, and N. A. Mendis, *J. Geophys. Res.* **90**, 7405 (1985).
- ²⁰H. L. F. Houpis and E. C. Whipple, *J. Geophys. Res.* **92**, 12507 (1987).
- ²¹O. Havnes, G. E. Morfill, and C. K. Goertz, *J. Geophys. Res.* **89**, 10999 (1984).
- ²²H. Ikezi, *Phys. Fluids* **29**, 1764 (1986).
- ²³M. J. McCaughey and M. J. Kushner, *Appl. Phys. Lett.* **55**, 951 (1989).
- ²⁴S. C. Lin and J. N. Bardsley, *J. Chem. Phys.* **66**, 437 (1977).
- ²⁵L. Schott, in *Plasma Diagnostics*, edited by W. Lochte-Holtgreven (North Holland, Amsterdam, 1968), pp. 668-731.
- ²⁶M. Hartig and M. J. Kushner, 43rd Gaseous Electronics Conference, Paper AA-4, Champaign, IL, 1990.
- ²⁷W. F. Ames, *Numerical Methods for Partial Differential Equations* (Academic, New York, 1977), pp. 119-134.
- ²⁸F. Kannari, M. Obara, and T. Fujioka, *J. Appl. Phys.* **57**, 4309 (1985).
- ²⁹T. J. Sommerer, M. S. Barnes, J. H. Keller, M. J. McCaughey, and M. J. Kushner (unpublished).
- ³⁰M. S. Barnes, J. H. Keller, J. C. Forster, J. A. O'Neill, and D. K. Coultas (unpublished).